Vietnam Journal of Catalysis and Adsorption
Tạp chí xúc tác và hấp phụ Việt Nam

https://jca.edu.vn

High efficiency of CQDs/UiO-66 photocatalytic nanocomposite for degradation of RR-195 under visible irradiation

Nguyen Thi Phuong Lan[1], Nguyen Thi Hong Van[2,3], Duong Thi Thuy Trang[4], Xuan Nui Pham[4,*]

[1] *Faculty of Applied Sciences, University of Economics-Technology for Industries, 456-Minh Khai, Vinh Tuy, Hai Ba Trung, Hanoi, Vietnam.*
[2] *Graduate University of Science and Technology, Vietnam Academy of Science and Technology, 18 Hoang Quoc Viet street, Cau Giay, Hanoi, Vietnam*
[3] *Institute of Environment, Vietnam Maritime University, 484 Lach Tray, Le Chan, Hai Phong, Vietnam*
[4] *Department of Chemical Engineering, Hanoi University of Mining and Geology, 18-Pho Vien, Duc Thang, Bac Tu Liem District, Hanoi, Vietnam.*
** Email: phamxuannui@humg.edu.vn*

ARTICLE INFO

Received: 12/02/2024
Accepted: 12/04/2024
Published: 30/12/2024

Keywords:
CQDs; UiO-66; degradation; RR-195; photocatalyst; nanocomposite

ABSTRACT

CQDs, characteristically quasispheroidal carbon nanoparticles composed of amorphous to crystalline carbon base, are a prospective semiconductor quantum dots owing to its excellent optical absorptivity, chemical stability, nontoxicity, and facile synthesis. In this study, we demonstrated the impregnation method to integrate CQDs, formed from chitosan with UiO-66 from terephthalic acid recycled by waste PET to synthesize CQDs@UiO-66 nanocomposite. After the hybridization of CQDs with UiO-66, the low band gap energy of the CQDs@UiO-66 sample was determined at 2.4 eV, allowed the demonstration of photocatalytic activity under high visible light. This material was tested in the photodegradation of RR-195 dye and compared with the pristine components. The highest RR-195 degradation efficiency recorded when using the catalyst mass of 50 mg, dye concentration of 70 ppm after 4 h under visible light irradiation was 96% and the result rather maintained its performance (86,4%) after four cycles. These results could promote a new material circularity pathway to develop new semiconductors that can be used to protect water from further pollution.

Introduction

Recently, carbon quantum dots (CQDs), a new class of carbon nanoparticles, have attracted much attention as a prospective semiconductor quantum dot owing to its excellent optical absorptivity, chemical stability, nontoxicity, and facile synthesis [1,2]. CQDs are characteristically quasispheroidal carbon nanoparticles composed of amorphous to crystalline carbon base. It is primarily made up of sp^2-graphitic carbon (or) graphene and graphene oxide sheets combined through the insertion of sp^3-hybridized carbon that exhibits fluorescence properties [3]. Moreover, physicochemical properties of CQDs, such as the solubility of CQDs in water and surface functionalization,... it can be easily modified due to the presence of various functional groups on their surfaces such as hydroxyl, carboxyl, ester, ether or amino with inorganic, organic polymeric or biological species. For example, CQDs prepared from chitosan was not only

https://doi.org/10.62239/jca.2024.065

rich in C atoms but it also contains numerous -OH and-NH_2 groups as well as amino glucose and N-acetylamino glucosemers linked by glycosidic bonds, applying widely in medicine and pharmacy as a three-dimensional scaffold in wound dressings or elements of controlled drug delivery and release systems [4]. Especially, their photoluminescent properties are not only size- and shape-dependent. As edge shapes, surface ligands and defects also play significant roles in determining their final characteristics as well as their photoluminescence depends on excitation wavelength (when CQDs are excited by UV to VIS, their emission wavelengths range from the UV to the near-IR region) [5]. Therefore, CQDs, potential replacement for the toxic metal-based quantum dots, are being used in various fields of applications such as bioimaging, medical diagnosis, biosensing, chemical sensing, photocatalysis, and photovoltaic devices [6].

Working as a cocatalyst, CQDs can play a versatile role such as an electron receptor, a photosensitizer, and/or a spectral converter, depending on the specific photocatalytic system. Therefore, CQDs have been intensively applied to combine with some inorganic photocatalysts and their application as a localized electron acceptor inside a MOF particles are to expand photosensitizers under long wavelength light irradiation of photocatalyst [7]. Metal–organic frameworks (MOFs) are a class of porous crystalline materials assembled from metal ions (or clusters) and organic linkers, featuring well-defined pore structures, high surface area and opened channels. When employed as photocatalysts, MOF materials can offer tremendous and dispersive active sites that are accessible to substrates/products via the opened channels. Furthermore, each active site (e.g., metal-oxo cluster) in MOFs can be regarded as a single quantum dot, serving as a light absorber, a charge generator, and a catalytic site like a small semiconductor [8]. Moreover, the organic linkers in MOFs can work as antennas to absorb extra ultraviolet (UV) light and transfer energy to the active sites via the ligand-to-metal charge transfer (LMCT) process [9].

Recently, some researchers reported to generate CQDs inside typical MOF photocatalysts to make prominent materials. Rongbin Lin et al. [10] embedded the CQDs into MIL-53(Fe) particles, which exhibit giant activity enhancement toward Cr(VI) reduction, while Chen et al. [11] had the smart integration of double superiorities of MOF and CQD guarantees the superior thermal features of pristine MOF-based PCMs, and further results in novel high-intensity fluorescence function with excellent color stability, thus satisfying the specific multifunctional requirements in particular devices, such as LEDs. Whereas Wei et al. [12] proposed the photocatalytic activity of CQDs/ZIF-8 composite under visible light was tested by removing gaseous NO in continuous air flow. Yu et al. [13] using CQDs/UiO-66 metal-organic-frameworks (MOG) composites (CQD/UiO-66 MOG) for photocatalytic degradation of toluene under visible light.

In recent research, we have developed some MOF materials which use BDC recycling from PET waste which has led to serious environmental pollution problems because of their poor biodegradability as a key ingredient for synthesis of MIL-101(Cr) [14], MIL-101(Fe) [15]. UiO-66 has emerged as a promising membrane material due to their exceptional stability as well as high connectivity to form and ensure the structural stability from the kinetic aspect.

From this inspiration and above overview study, we proposed the use of terephthalic acid produced from recycled plastic bottles and chitosan as cheaper sources for the synthesis of UiO-66 and CQDs, respectively. After that, these pristine materials were integrated into nanocomposite CQDs@UiO-66 which is the new structure of material for enhancing of photocatalyst ability. CQDs@UiO-66 was tested in the photodegradation of RR-195 and was compared with the pristine components.

Experimental

Materials

Zirconi chloride ($ZrOCl_2.8H_2O$), chitosan (deacetylation degree $C_6H_{11}NO_4$ 82.5%), terephthalic acid (H_2BDC 99.8%), sodium hydroxide (NaOH, 98%), sulfuric acid (H_2SO_4, 98%), acetic acid (CH_3COOH, 99%), hydrogen peroxide (H_2O_2, 30%), dimethylformamide (DMF, 99.8%), ethylene glycol (EG, 99%), methanol (CH_3OH), ethanol (C_2H_5OH), deionized water and polyethylene terephthalate (PET) as well as water bottles were collected from the Hanoi University of Mining and Geology campus. After the removal of caps, labels and gaskets, the cleaned objects were cut into small pieces by manual scissors, synthesized TPA.

Recovery of TPA from PET

Terephthalic acid (TPA) employed was recycled from polyethylene terephthalate plastic bottles using the synthetic procedure reported previously [15]. First, dissolve polyethylene terephthalate (PET) in a mixture of ethylene glycol (EG) and NaOH. Then heat at 180°C

https://doi.org/10.62239/jca.2024.065

and stir continuously for 3 h until a homogeneous solution is obtained. From that homogeneous solution, add 2 M H_2SO_4 solution slowly to obtain a white precipitate. Filter and wash the precipitate several times with distilled water until pH=7. Finally, the precipitate was dried at 100°C for 24 h, and a fine white powder called TPA was obtained.

Synthesis of UiO-66

UiO-66 was synthesized according to the procedure of Abida *et al.* [16]. Briefly, 0.997 grams of terephthalic acid was dispersed in 200 mL DMF by a magnetic stirrer for 5 hours, then sonicating for 30 minutes to form a homogeneous solution (solution A). 0.35 grams of $ZrOCl_2.8H_2O$ was completely dissolved in 15 mL of DMF after magnetic stirring for 3 h, then sonicating for 30 min. From that solution, add 0.324 mL deionized water, 1.351 grams acetic acid, use a sonicator for 30 mins to dissolve and stir for 24 h (solution B). After that, drop slowly 5 mL solution A from burette into solution B, stir at room temperature then put it into a Teflon-lined stainless-steel autoclave to enhance the attached ability of materials heated up to 120°C for 36 h.

Then, wash the sample with 50 mL DMF at 70°C for 3 times with 3 h each time, and with 50 mL C_2H_5OH at 60°C for 3 h. After each stirring period, centrifugally spin to completely remove impurities. Finally, these samples will be dried at 100°C for 24 h and obtain UiO-66–a white powder.

Synthesis of CQDs

The CQDs were prepared by the hydrothermal method using chitosan as a precursor according to the method reported by Yang [17]. The typical synthesis is described as follows: firstly, 0.5 g of chitosan was added to 100 mL of 1% acetic acid solution and dissolved at room temperature using ultrasonic technique, and then the prepared chitosan solution was filtered to remove the insoluble substance. Secondly, the solution was placed in an autoclave (50 mL) and heated at 180°C for 12 h. Thirdly, when cooled down to room temperature, the brownish black solution was filtered. Next the solution was centrifuged at 10000 rpm for 15 min to remove all deposits and yield a canary yellow CQD aqueous solution, and then the as-prepared CQDs were stored in a refrigerator at 4°C for future use. The final CQDs were denoted as CHI-12, where 12 referred to the carbonization time.

Synthesis of CQD@UiO-66 nanocomposite

CQDs@UiO-66 nanocomposite materials were synthesized by impregnation method. CQDs are fixed on the surface of UiO-66 according to the following procedure: 0.1 g of UiO-66 was dispersed in 20 mL methanol stirred for 30 min, then add of 5 mL CQDs solution into suspension dropwise and stir for 2 h. The mixture was soaked in an ice bath for 30 minutes. The suspension was magnetically stirred at room temperature for 24 h to reach adsorption equilibrium. The final product was obtained by centrifugation and filtered, washed with deionized water three times, and dried naturally.

Characterisation

The crystal lattice structure of the synthesized samples was determined by X-ray powder diffraction (XRD) using a D8 ADVANCE system (Cu Ka1 copper radiation, λ = 0.154 nm, 3° min-1 scanning speed, Bruker, Germany). The UV-vis diffuse reflectance (DRS-UV) and photoluminescence (PL) spectra were performed with the UV-2600 spectrophotometer (Shimadzu) and the Cary Eclipse fluorescence spectrophotometer (Varian), respectively. Surface morphology was observed by a scanning electron microscope (S-4800, Hitachi). The Fourier transform infrared spectra (FT-IR) were measured with an FT-IR Affinity-1S (SHIMADZU).

Photocatalytic experiments

The photocatalytic activity of CQDs@UiO-66 materials was evaluated by decomposition of Reactive Red 195 (RR-195) dye in water using sunlight. In the experiment, 50 mg of the catalyst was dispersed in RR-195 solution (30 mL, 50 ppm). Before sunlight irradiation, the mixture was magnetically stirred for 60 min to reach adsorption-desorption equilibrium. After 1 h, the mixture was exposed to sunlight, at fixed intervals, 5 mL of the solution sample was removed, centrifuged to remove solids. The solution fraction was analyzed using a UV-Vis 2450 spectrophotometer at a maximum absorption peak of 541 nm. The initial solution concentration is called C_o, the solution concentration after each time interval is C_t. The decomposition efficiency is calculated by the formula:

$$\%H = \frac{C_o - C_t}{C_o}.100$$

Results and discussion

Characterisations of materials

Figure 1 shows that XRD patterns of UiO-66 was recorded two main peaks at angle 2θ=7.34; 8.48° corresponds to the diffraction planes (111); (200) which can match the result of previous research that

synthesized UiO-66 [18, 19]. The diffraction peak of sample UiO-66 has high intensity, sharpness, and sharpness; typically, a major peak at the 7.34° position (characteristic for this material), indicating high crystallinity. For nanocomposite samples, the characteristic peaks of UiO-66 were still preserved, but the intensity of the peaks decreased. This could be due to CQDs were evenly dispersed on the surface of the UiO-66 crystal, resulting in a decrease in the crystallinity of the UiO-66 particles.

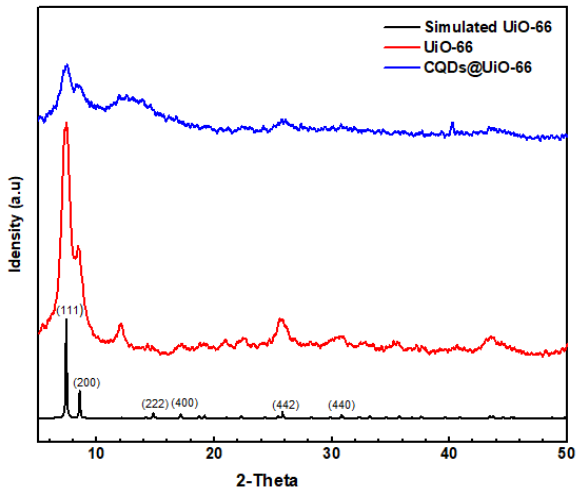

Fig. 1: XRD patterns of UiO-66 and CQD@UiO-66

FT-IR spectroscopy was performed to detect chemical compositions and sample bonding. The FT-IR spectra of UiO-66 and CQDs@UiO-66 are shown in Fig 2, where pure UiO-66 exhibits characteristic absorption peaks at 3300; 1653; 1577; 1506; 1398; 814; 746; 667 cm^{-1}. For UiO-66 (Zr), the two high-intensity bands at about 1577 and 1398 cm^{-1} correspond to the asymmetric and symmetric stretching oscillations of the carboxylate group (RCO_2^-) in the BDC^{2-} ligands, respectively, are consistent with the expected values for the synaptic, syn-chelating mode. The weak band at about 1506 cm^{-1} corresponds to the stretching oscillations of the C=C bonds in the aromatic ring, while at lower wave numbers the band around 746 cm^{-1} can be associated with the C-H bending mode. Furthermore, the remarkably strong band around 525 cm^{-1} is a consequence of the asymmetrical stretching mode of Zr–[OC], and the bands around 667 and 475 cm^{-1} are probably largely due to stretching in μ_3-O and μ_3-OH group, respectively [12, 20]. Furthermore, a band corresponding to the C=O asymmetric stretching of the DMF can be observed at 1653 cm^{-1}, demonstrating that the DMF is located in the pores.

CQDs@UiO-66 has a strong absorption in the range 3200–3400 cm^{-1}, which is observed corresponding to the stretching of –OH, which proves that the surface of CQDs contains -OH. The characteristic peaks for C–O, –COOH and –OH observed at the same wavelength of CQDs@UiO-66 also show that the prepared CQDs have many surface hydroxyl groups and are readily soluble in water.

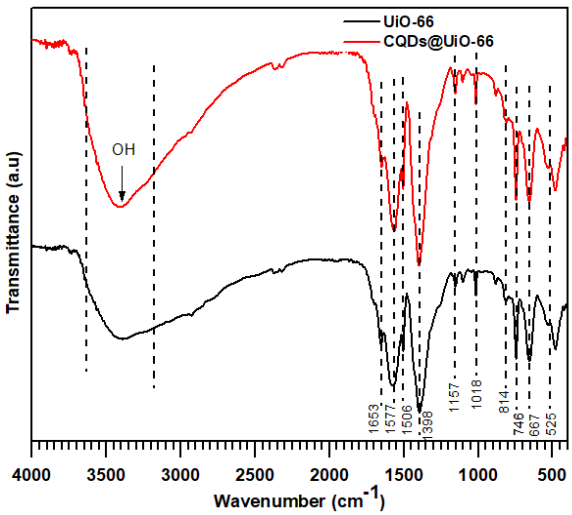

Fig. 2: FT-IR spectra of UiO-66 and CQDs@UiO-66

The scanning electron microscopy (SEM) images in Figure 3(a),(b) show that UiO-66 had fairly uniform shapes and structures, the morphology of UiO-66 consisted of regular octahedral crystals with a smooth face. The presence of CQDs after being doped on UiO-66 in Fig. 3(c),(d) showed that CQDs were evenly dispersed on the surface of UiO-66. The particle size of CQDs was 10 nm.

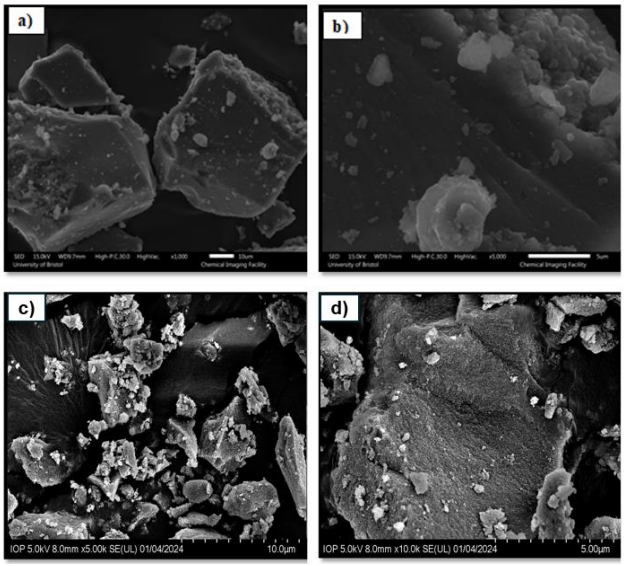

Fig. 3: Images SEM of (a), (b) UiO-66 and (c),(d) CQDs@UiO-66

Optical properties

The band-gap energies of the samples could be estimated by Tauc's plots: $(\alpha h\nu) = A(h\nu - Eg)^{n/2}$, *where* α, *h*, *ν*, *A*, and *Eg* are indicative to the absorption coefficient, Planck's constant, light frequency, constant value, and band-gap energy, and n is 1 to 4 for a direct and indirect band-gap semiconductor, respectively.

In Fig 4(a), UiO-66 exhibits strong absorption in the visible light range, so this material can capture visible light potentially. The absorption edge of CQDs@UiO-66 is observed at about 470 nm. Therefore, the enhancement of visible light absorption in CQDs@UiO-66 nanocomposites has been suggested due to the resonance effect between UiO-66 and CQDs.

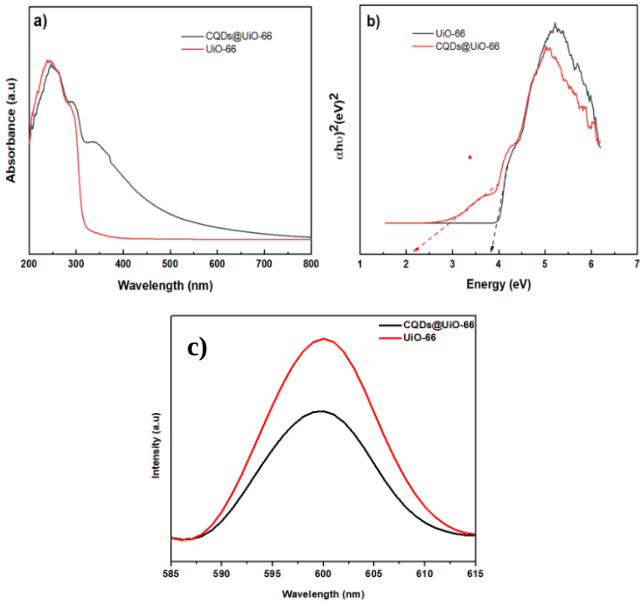

Fig. 4: (a) UV-Vis diffuse reflectance spectra; (b) band gap; and (c) photoluminescence (PL) spectra of the UiO-66 and CQDs@UiO-66 composites

The plot of $(\alpha h\nu)^{1/2}$ versus hν (eV) of UiO-66 and CQDs@UiO-66 are shown in Fig 4(b). The band gap energies of the samples CQDs@UiO-66, UiO-66 were calculated and estimated to be 2.4 eV and 3.8 eV, respectively. CQDs@UiO-66 have the lowest Eg (2.4 eV), which proves that the ability of this material to absorb visible light is better than the other samples.

In Fig 4c, the PL emission peak of UiO-66 was at 600 nm and has the highest emission intensity, representing the rapid recombination of the photogenerated electron-hole pairs. The emission intensity of the CQDs@UiO-66 photocatalyst was much lower than that of UiO-66, which is beneficial for the separation of charge carriers, implying that the efficient separation of photochargers beneficial to enhance photocatalytic activity and increase the efficiency of pollutant treatment.

Photocatalytic activity

In Fig 5, the degradation efficiency of RR-195 of the composite after 4 h is 99.7%, while the one of RR- 195 after the same time of UiO-66 is 96.3%. The CQDs@UiO-66 composite may perform better in the visible light region, leading to excitation for generation of many photogenerated electron-hole pairs, on the other hand, with the advantage of the surface and capillary as well as the structure makes the decomposition of RR-195 under artificial light highly efficient.

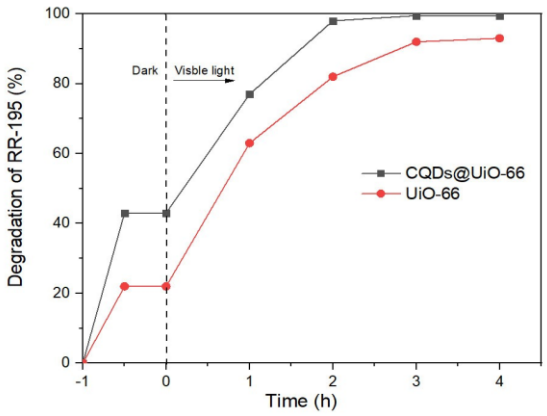

Fig. 5: Effect of photocatalysts on the degradation of dye RR-195

Figure 6a shows the result of studying the effect of photocatalyst mass on the degradation of RR195. In fact, the highest photocatalytic efficiency reached 99.7% after 4 h corresponding to 50 mg of catalyst and then the efficiency tended to decrease when increasing the amount of catalyst to 70 mg. With a large amount of catalyst, the formation of active sites will increase, and the production of free electrons in the conduction band. However, when the amount of catalyst was too high, it will cause interactions between the surface layers of the material, reducing the formation of the inner hole photoelectron layers leading to a decrease in the photocatalytic efficiency [17]. Therefore, 50 mg of CQDs@UiO-66 was used for the subsequent RR-195 dye degradation experiments.

Fig. 6b, about 99% of RR-195 decomposes when H_2O_2 was used, while about 98% of RR-195 was decomposed without H_2O_2. Therefore, the photocatalytic activity of CQDs@UiO-66 materials did not change at all much in the presence and absence of H_2O_2. It may be interpreted that oxygen atom doping has significantly improved the separation efficiency of electron and hole pairs on the catalyst. It shows that the use of H_2O_2 is not necessary in the degradation of dye RR-195.

At the same condition as the above experiment, the influence of the concentration of CQDs@UiO-66 on the

https://doi.org/10.62239/jca.2024.065

photodegradation of RR195 is shown in Fig 6c. The content of CQDs has a great influence on the photocatalytic performance of the materials. 5 mL of CQDs, the highest photocatalytic activity, was possible to degrade RR-195 to 99.1% after 4 h of irradiation. While the sample using 7 mL of CQDs, the decomposition efficiency of RR-195 reached 95.6% after 4 h of light. This may be due to the excess CQDs clump together, preventing the photogenesis of electron-hole formation.

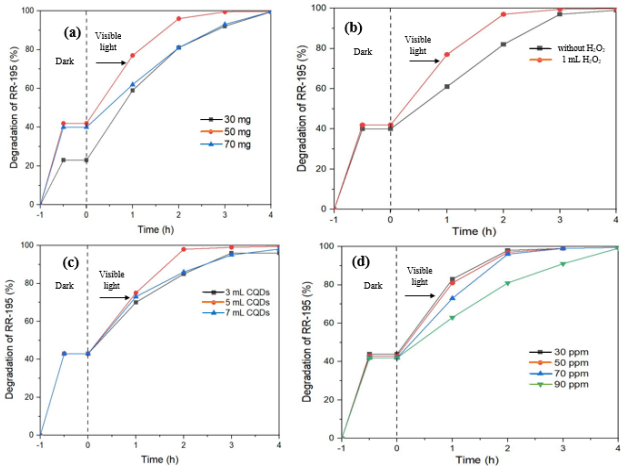

Fig. 6: Photodegradation of RR-195 using CQDs@UiO-66 catalyst (a) various amounts; (b) with and without H_2O_2; (c) various volumes of CQDs (0.5% wt.); (d) various concentration of RR-195

The degradation of RR-195 on CQDs@UiO-66 catalyst was investigated by varying the initial concentration of RR-195 while maintaining a constant amount of catalyst (50 mg). As can be seen in Fig 6d, the photodegradation efficiency decreased from 99.9% to 99.4% when the initial concentration of RR-195 was increased from 30 to 90 ppm. Theoretically, more RR-195 molecules could be adsorbed on the catalyst surface as the initial concentration of RR-195 increased, however there would be fewer free sites on the catalyst surface for receive photons and reduce the rate of light transmission into the dye solution. Its intermediates in the degradation can inhibit the further photocatalytic degradation of RR-195. Thus, the addition of CQDs on UiO-66 substrate not only increases the conversion effect but can also generate oxygen vacancies in the substrate [21], which increases light absorption and charge separation under visible light, and easily facilitates the generation the generation of active species of $O_2^{\cdot-}$ radicals. Therefore, the photocatalytic degradation efficiency of RR-195 has been improved [22].

To evaluate the stability and regeneration ability of CQDs@UiO-66, the degradation of dye RR-195 using CQDs@UiO-66 photocatalyst was repeated 4 times. The obtaned results show that CQDs@UiO-66 is a stable photocatalyst and the photocatalytic decomposition efficiency still reaches 86.4% after four cycles. That proves the efficiency and durability of CQDs@UiO-66 composite photocatalysts.

Conclusion

CQDs@UiO-66 photocatalytic nanocomposite was synthesized by a green synthesis using chitosan and waste PET as raw material sources. By physicochemical analysis methods such as XRD, FT-IR, SEM, UV-Vis-DRS and PL spectroscopy. The obtained results show the morphology of UiO-66 consisted of regular octahedral crystals with a smooth face and CQDs were evenly dispersed on the surface of UiO-66. The bandgap energies of CQDs@UiO-66 was estimated to be 2.4 eV lower than that of pure UiO-66. The photocatalytic activity of CQDs@UiO-66 photocomposite shows that the degradation efficiency of RR-195 reaches 99% under optimal conditions, including: 50 mg of CQDs@UiO-66 mass, 50 ppm of initial concentration of dye RR-195 in 4 h of reaction time under visible irradiation.

Acknowledgments

The authors would like to thanks the financial support of the 2023-2024 project from University of Economics–Technology for Industries.

References

1. S. Chaudhary, S. Kumar, B. Kaur, S.K. Mehta, RSC Adv. 6 (2016) 90526-90536. https://doi.org/ 10.1039/c6ra15691f
2. K. Qu, J. Wang, J. Ren, X. Qu, Chem. - A Eur. J. 19 (2013) 7252. https://doi.org/ 10.1002/chem.201300042
3. P. Singh, A. Borthakur, P. K Mishra, D. Tiwary, Nano-Materials as Photocatalysts for Degradation of Environmental Pollutants, Challenges and Possibilities, 2019. https://doi.org/10.1016/C2018-0-03858-X
4. Ł. Janus, M. Piątkowski, J. Radwan-Pragłowska, D. Bogdał, D. Matysek, Nanomaterials 9 (2019) 274. https://doi.org/10.3390/nano9020274
5. Z. Li, G. Che, W. Jiang, L. Liu, H. Wang, RSC Adv. 9 (2019). https://doi.org/10.1039/c9ra05600a
6. J. Yu, X. Wang, L. Chen, G. Lu, G. Shi, X. Xie, Y. Wang, J. Sun, Chem. Eng. J. 435 (2022) 135033. https://doi.org/10.1016/j.cej.2022.135033
7. P.S. Bárcia, D. Guimarães, P.A.P. Mendes, J.A.C. Silva, V. Guillermc, H. Chevreau, C. Serre, and A.E. Rodrigues,

Micropor. Mesopor. Mat. 139 (2011) 67–73. https://doi.org/10.1016/j.micromeso.2010.10.019

8. A.M. Viana, S.O. Ribeiro, B. Castro, S.S. Balula, L. Cunha-Silva, Materials 12 (2019) 3009. https://doi.org/10.3390/ma12183009
9. X. Zhou, W. Huang, J. Shi, Z. Zhao, Q. Xia, Y. Li, H. Wang, Z. Li, J. Mater. Chem. A. 2(13) (2014), 4722–4730. https://doi.org/10.1039/C3TA15086K
10. R. Lin, S. Li, J. Wang, J. Xu, C. Xu, J. Wang, C. Li, Z. Li, Inorg. Chem. Front. 5 (2018) 3170–3177. https://doi.org/10.1039/C8QI01164H
11. X. Chen, H. Gao, M. Yang, L. Xing, W. Dong, A. Li, H. Zheng, G. Wang, Energy storage mater. 18 (2018) 349–355. https://doi.org/10.1016/j.ensm.2018.08.015
12. X. Wei, Y. Wang, Y. Huang, C. Fan, J. Alloys and Comp. 802 (2019) 467–476. https://doi.org/10.1016/j.jallcom.2019.06.086
13. J. Yu, X. Wang, L. Chen, G. Lu, G. Shi, X. Xie, Y. Wang, J. Sun, Chem. Eng. J. 435 (2022) 135033. https://doi.org/10.1016/j.cej.2022.135033
14. X.N. Pham, V.-T. Vu, H.V.T. Nguyen, T.-T.-B. Nguyen, H.V. Doan, Nanoscale Adv. 4 (2022) 3600–3608. Htttps://doi.org/10.1039/d2na00371f
15. N.T. Hoa, L.T. Nguyen, V.V. Tai, X.N. Pham, Vietnam Journal of Catalysis and Adsorption, 10 (2021) 125–136. https://doi.org/10.51316/jca.2021.079
16. H.R. Abida, H. Tian, H.-M. Anga, M.O. Tadea, C. Buckley, S. Wang, Chem. Eng. J., 187 (2012) 415–420. https://doi.org/10.1016/j.cej.2012.01.104
17. Y. Yang, J. Cui, M. Zheng, C. Hu, S. Tan, Y. Xiao, Q. Yang, Y. Liu, Chem. Commun. 48 (2012) 380–382. https://doi.org/10.1039/C1CC15678K
18. H. R. Abid, G. H. Pham, H. M. Ang, M. O. Tade, S. Wang, J. Colloid Interf. Sci. 366 (2012) 120–124. https://doi.org/10.1016/j.jcis.2011.09.060
19. A.M. Viana, S.O. Ribeiro, B. Castro, S.S. Balula, L. Cunha-Silva, Materials 12 (2019) 3009. https://doi.org/10.3390/ma12183009
20. P.S. Bárcia, D. Guimarães, P.A.P. Mendes, J.A.C. Silva, V. Guillermc, H. Chevreau, C. Serre, A.E. Rodrigues, Micropor. Mesopor. Mat. 139 (2011) 67–73. https://doi.org/10.2016/J.MICROMESO.2010.10.019
21. N. Prasetya, B.P. Ladewig, J. Mater. Chem. A 7 (2019) 15164–15172. https://doi.org/10.1039/C9TA02096A
22. J. Yu, X. Wang, L. Chen, G. Lu, G. Shi, X. Xie, Y. Wang, J. Sun. Chem. Eng. J. 435 (2022) 135033. https://doi.org/10.1016/j.cej.2022.135033